Cell Tissue Res (1999) 295:111-120

REGULAR ARTICLE

Geoff R. Newman · Lee Campbell · Chris von Ruhland
Bharat Jasani · Mark Gumbleton

Caveolin and its cellular and subcellular immunolocalisation in lung alveolar epithelium: implications for alveolar epithelial type I cell function

Received: 6 March 1998 / Accepted: 21 July 1998

Abstract Caveolae are flask-shaped invaginations of the plasmalemma which pinch off to form discrete vesicles within the cell cytoplasm. Biochemically, caveolae may be distinguished by the presence of a protein, caveolin, that is the principal component of filaments constituting their striated cytoplasmic coat. Squamous alveolar epithelial type I (ATI) cells, comprising approximately 95% of the surface area of lung alveolar epithelium, possess numerous plasmalemmal invaginations and cytoplasmic vesicles ultrastructurally indicative of caveolae. However, an ultrastructural appearance does not universally imply the biochemical presence of caveolin. This immunocytochemical study has utilised a novel application of confocal laser scanning and electron microscopy unequivocally to localise caveolin-1 to ATI cells. Further, cytoplasmic vesicles and flask-shaped membrane invaginations in the ATI cell were morphologically identified whose membranes were decorated with anti-caveolin-1 immunogold label. Coexistent with this, however, in both ATI and capillary endothelial cells could be seen membrane invaginations morphologically characteristic of caveolae, but which lacked associated caveolin immunogold label. This could reflect a true biochemical heterogeneity in populations of morphologically similar plasmalemmal invaginations or an antigen threshold requirement for labelling. The cuboidal alveolar epithelial type II cell (ATII) also displayed specific label for caveolin-1 but with no ultrastructural evidence for the formation of caveolae. The biochemical association of caveolin with ATI cell vesicles has broad implications for the assignment and further study of ATI cell function.

G. R. Newman · C. von Ruhland
Medical Microscopy Sciences Unit, University of Wales College of Medicine, Cardiff, CF4 4XN, UK

L. Campbell · M. Gumbleton (✉)
Welsh School of Pharmacy, Cardiff University, Cardiff, CF1 3XF, UK
Tel.: +44 1222 874000, ext 5449; Fax: +44 1222 874159;
e-mail: gumbleton@cardiff.ac.uk

B. Jasani
Immunocytochemistry and Molecular Pathology Unit, University of Wales College of Medicine, Cardiff, CF4 4XN, UK

Key words Caveolin · Caveolae · Lung · Alveolar epithelial type I cell · Immunocytochemistry · Electron microscopy · Confocal laser scanning microscopy · Rat (CD)

Introduction

Caveolae are flask-shaped invaginations connected by a neck-like structure to the plasmalemma presenting an opening to the extracellular space of diameter 20–40 nm. Despite suggestions that the membranes of caveolae invaginations remain continuous with the plasmalemma (Bungard et al. 1979), thereby providing a spatial continuity with the cell exterior, sufficient functional data have now been obtained to indicate that at least certain populations can detach to form discrete cytoplasmic caveolae vesicles of diameter 80–100 nm (Kurzchalia and Parton 1996; Parton et al. 1994). Reported caveolae functions include: the concentrating and internalisation of small molecules or ions by the process of potocytosis (Anderson et al. 1992), and serving as a localising domain within the plasma membrane for a range of signal transduction molecules (Wu et al. 1997 and reviews of Lisanti et al. 1994 and Couet et al. 1997). Caveolae are also recognised to act as intracellular trafficking (Fielding and Fielding 1996), and endocytotic and transcytotic, vesicles for macromolecules (Schnitzer and Oh 1994).

The morphologic features of caveolae have been recognised for many years (Fawcett 1966) and are most prominent in adipocytes and smooth muscle, fibroblast and capillary endothelial cells. However, it is only comparatively recently that biochemical distinction of caveolae from other non-clathrin-coated invaginations and free cytoplasmic vesicles has been possible and, as a corollary, the formulation of caveolae function derived from studies conducted in a range of different cell phenotypes. At the electron-microscopic level caveolae invaginations lack the electron-dense cytoplasmic coat characteristic of clathrin-coated pits. Biochemically caveolae have been distin-

guished from other 'non-coated' invaginations/vesicles by the presence of caveolin, a 21–24 kDa integral membrane protein, which is the principal component of filaments that constitute their striated cytoplasmic coat (Rothberg et al. 1992; Glenney and Soppet 1992). Caveolin protein itself remains membrane attached at both the plasmalemma invagination and discrete cytoplasmic caveolae vesicle stages. The interaction between oligomeric caveolin complexes and membrane lipids (Monier et al. 1996) fulfils a critical role in the generation of caveolae structure. The caveolin family constitutes at least three distinct genes encoding four caveolin proteins (Couet et al.1997): caveolin-1 isoforms α and β (24 and 21 kDa, respectively); caveolin-2 (21 kDa) (Scherer et al. 1996), and the muscle-specific form caveolin-3 (21 kDa) (Way and Parton 1995; Tang et al. 1996; Song et al. 1996). Prior to 1996, caveolin studies in the literature conducted in non-muscle-derived cells relate to the protein product that has subsequently been defined as caveolin-1.

The morphologic membrane features suggestive of caveolae invaginations are recognised in electron-microscopic (EM) images of squamous alveolar epithelial type I cells (ATI), the cell type constituting 93–95% of the surface area of the alveolar epithelium (Crapo et al. 1982; Haies et al. 1981). Indeed, it has been estimated (Gil 1983) that 70% of the surface area of the ATI cell plasmalemma is located within such invaginations. However, defining caveolae by ultrastructural appearance alone is not sufficient for considering potential function, the latter necessitating structural association with caveolin. The biochemical characterisation of the ATI plasmalemmal invaginations/cytoplasmic vesicles has so far not been reported. The aim of this present study was therefore to confirm immunocytochemically that the invaginations/cytoplasmic vesicles in the ATI cell in vivo are associated with immunoreactivity to caveolin, i.e., conform to the biochemical definition of caveolae. The biochemical confirmation of ATI cell vesicles as caveolae has broad implications for the assignment and study of potential ATI cell functions.

Materials and methods

Male pathogen-free rats (CD strain) of body weight 120–180 g were used throughout. The rats were bred and maintained in controlled temperature and lighting under barrier conditions with access to food and water ad libitum. Animal experiments were conducted in compliance with the animal (Scientific Procedures) Act 1986.

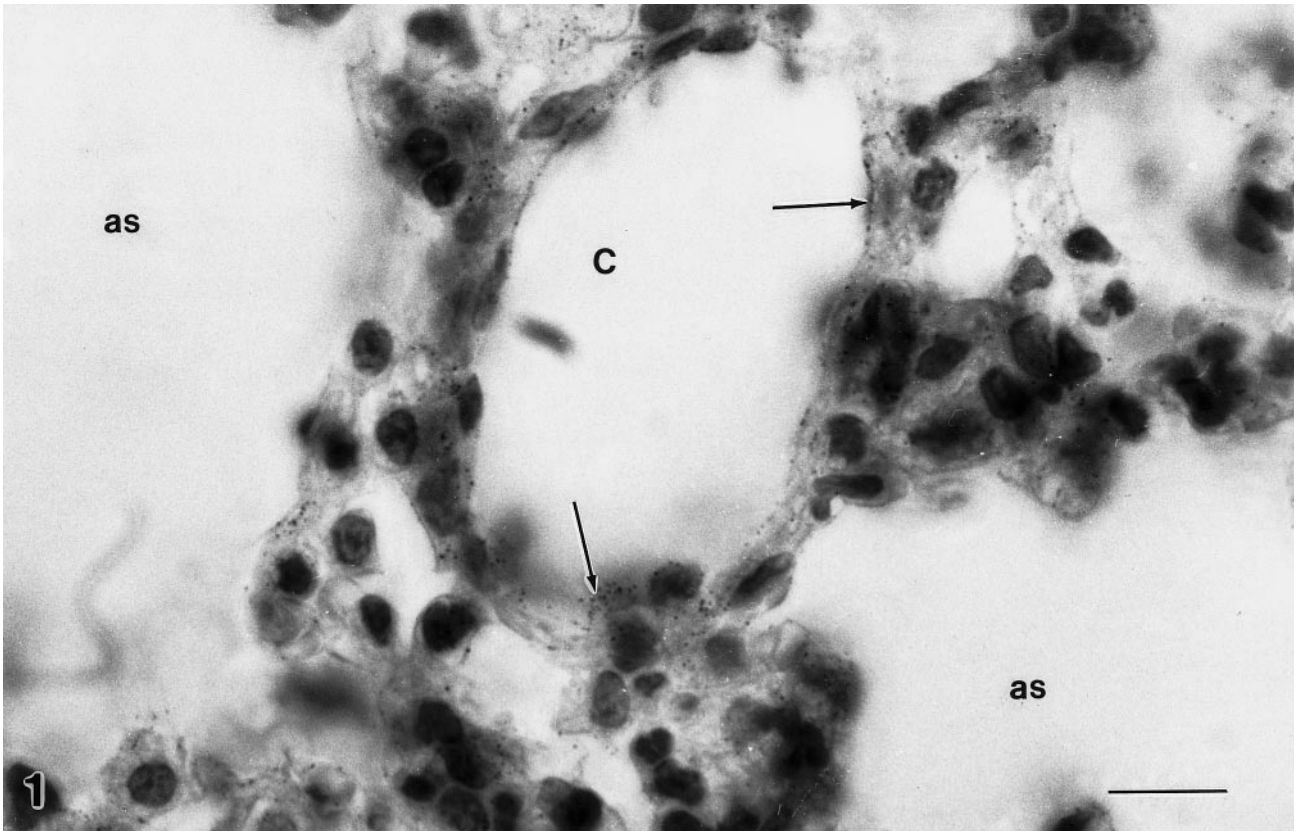

Fig. 1 Bright-field light micrograph of a 10-μm-thick paraffin section of glutaraldehyde perfusion-fixed rat lung immunostained with anti-caveolin antibody and immunocolloidal gold. The colloidal gold has been visualised by silver development and can be seen most prominently along the endothelial side of a centrally located blood vessel (*arrows*). Peripherally, various air-spaces are surrounded by profiles of alveolar epithelium and vascular endothelium. The section is lightly counterstained with haematoxylin to show nuclear structure (*as* air space, *C* capillary lumen). *Scale bar* 20 μm

Isolation and perfusion fixation of lung tissue

Lung tissue was fixed by a whole-body perfusion method as briefly described previously (Yohimura et al. 1986). Under terminal anaesthesia with halothane the pulmonary vasculature was perfused with a prewarmed (37°C) balanced saline solution delivered at a hydrostatic pressure of 120 cm via a cannula inserted into the pulmonary artery. The left atrium was cut to allow outflow of perfusates. When the perfusate flowed free of blood, perfusion with highly purified 1% monomeric 0.1 M phosphate-buffered glutaraldehyde (pH 7.4) (TAAB Laboratories Equipment Ltd., Berks., UK) was initiated. The lungs were perfusion fixed in situ for 15 min with approximately 150 ml of fixative. Following perfusion fixation, 1–5 mm^3 tissue samples were dissected and immersed in the same fixative for a further 2 h. In order to facilitate complete fixation, air was removed from the lung pieces by placing them, whilst in the fixative, under vacuum using a pump developing 0.1 barr pressure (Model VP1, KNF Neuberger UK Ltd., Oxford, UK). The tissue blocks were then washed in several changes of 0.1 M phosphate buffer to remove excess fixative and stored at 4°C overnight.

Paraffin wax embedding of lung tissue

The following day tissue blocks were washed in double distilled water (ddH_2O, 2x15 min) to remove residual phosphate ions and some were dehydrated in an ethanol/xylene gradient and embedded in paraffin wax using a Shanndon (Shanndon, Cheshire, UK) automated tissue processor. Paraffin wax sections (5–10 μm) were cut from the resulting blocks and mounted on superfrost microscope slides (Shanndon) in preparation for either staining with haematoxylin and eosin, or immunostaining and counterstaining with haematoxylin or methyl green.

Immunostaining of paraffin wax sections

Following removal of paraffin, the slides containing the rehydrated sections were placed in a humidified chamber and, prior to antibody incubation, each section was equilibrated for 10 min in 100 μl 0.6% bovine serum albumin (BSA) in 0.01 M phosphate-buffered solution (PBS), pH 7.1 (PBS/BSA). After draining, the sections were covered for 1 h at room temperature in serial dilutions (1:500; 1:1000; 1:2000; 1:4000) of polyclonal anti-caveolin-1 antibody (host-rabbit; Transduction Labs, USA, distributed by Affinity, Mamhead, UK) made from the 0.25 μg/ml antibody stock solution. The diluent was 0.6% BSA in 0.01 M PBS. Further sections were included to act as controls in which the primary antibody was omitted or substituted with an inappropriate primary antibody. The sections were then washed 3x5 min with PBS and covered for 1 h with 100 μl goat anti-rabbit IgG antibody (Sigma, Poole, Dorset, UK) conjugated to 5-nm colloidal gold (manufactured in-house, Medical Microscopy Sciences Unit, UWCM, Cardiff, UK) diluted 1:40 in PBS/BSA. Sections were washed in PBS (3x3 min) and in ddH_2O (2x5 min) prior to silver amplification. Free aldehyde groups were blocked with 0.75 M TRIS acetate buffer pH 7.4 (3x2 min). The imperceptible immunocolloidal gold label was made visible in the light microscope with a new physical developer (Newman and Jasani 1998, in press) following which sections were counterstained with haematoxylin or methyl green.

Bright-field and confocal laser scanning microscopy

Coverslipped, immunostained rehydrated paraffin sections were photographed in a Reichert photomicroscope and analysed in a Leica TCS4D confocal laser scanning microscope (CLSM) fitted with a krypton/argon laser (Leica UK Ltd., Milton Keynes UK). The dense colloidal gold/silver immunostain provided a strong signal when the CLSM was set up in reflection mode. Using x40 and x100 oil-immersion lenses, various stacks of optical sections taken all the way through the tissue in the "z" plane were stored, usually at a sampling thickness of 0.3–0.4 μm and in a 512x512-pixel format, as electronic image data sets. These sets were then shown as galleries and reconstructed as extended focus views, stereo pairs or red/green stereo images over which CLSM transmission images could be ghosted to show background structures (Adobe Photoshop software, Adobe Systems Europe Ltd., Edinburgh, Scotland, UK).

Resin embedding of lung tissue

Some of the remaining ddH_2O-washed tissue blocks from the glutaraldehyde perfusion-fixed rat lung were postfixed in 2% neutrally buffered osmium tetroxide for 2 h and, following washing, infiltrated and embedded in Araldite by a routine method (Glauert 1991). Semithin (1 μm thick) resin sections were placed on droplets of water and dried onto superfrosted slides, where they were stained with haematoxylin and eosin, or 0.5% toluidine blue in 1% borax, for light microscope viewing and photography. Sections (70 nm thick) were mounted unsupported on the matt side of 300-mesh copper grids and contrasted with saturated uranyl acetate and Reynolds' lead citrate (Reynolds 1963).

The remaining lung tissue blocks were washed in ddH_2O as for the previous samples and postfixed in 2% aqueous uranyl acetate for 2 h in the dark; this was followed by 2x15-min washes in ddH_2O to remove excess uranyl acetate. The blocks were then partially dehydrated to 70% ethanol in a graded series of solutions for 2x15 min in each solution and embedded in LR White acrylic resin by the cold chemical catalytic method (Newman and Hobot 1987; Newman and Hobot 1993). Briefly, infiltration was initiated with a mixture of LR White resin (hard grade, precatalysed, London Resin Co., Basingstoke, UK) and 70% ethanol (2:1) for 1 h and completed with 3x30-min changes of LR White resin at room temperature. Finally, the tissue blocks were dropped into 0-gauge gelatin capsules containing LR White resin precooled to 0°C to which the manufacturer's accelerator had been added (1.5 μl accelerator/ml resin). The capsules were then tightly lidded and the resin left to polymerise overnight in the refrigerator at 0°C. LR White semithin sections were dried down from water droplets onto superfrosted slides and stained with haematoxylin and eosin or toluidine blue. Thin sections (70–90 nm) were mounted unsupported on the shiny side of 300-mesh, ethanol-washed, nickel grids ready for immunolabelling.

Immunolabelling of LR White sections

In a moist chamber, nickel grids containing the lung sections were immersed and allowed to equilibrate (2x20 min) in 20 mM TRIS buffer (pH 8.0) containing 1% BSA (TRIS/BSA). The grids were then immersed for 1 h in 50-μl droplets of polyclonal anti-caveolin-1 antibody at dilutions of 1:500, 1:1000, 1:2000 and 1:4000 in TRIS/BSA. Control grids were also included in which the primary antibody was omitted or substituted with an inappropriate antibody. After incubation the grids were rinsed in TRIS/BSA (3x1 min) and immersed for 1 h in 50-μl droplets of goat anti-rabbit IgG antibody conjugated to 10-nm colloidal gold particles diluted 1:5 with TRIS-BSA buffer. The grids were then rinsed in TRIS/BSA (2x1 min) and ddH_2O (3x1 min) before counterstaining in 2% uranyl acetate and Reynolds' lead citrate.

Electron-microscope viewing and photography of resin sections

Following contrasting or immunolabelling and counterstaining, all thin sections were viewed and photographed in a CM12 Philips transmission electron microscope at an accelerating voltage of 80 or 100 kV.

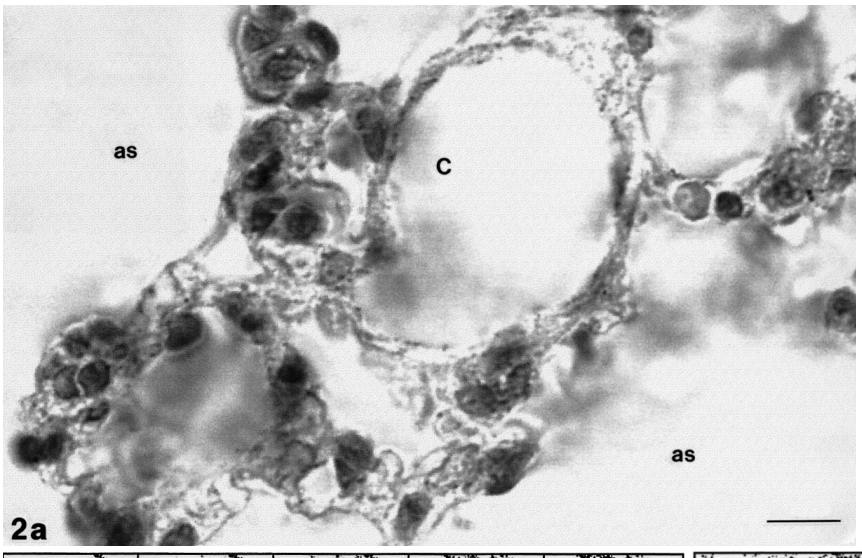

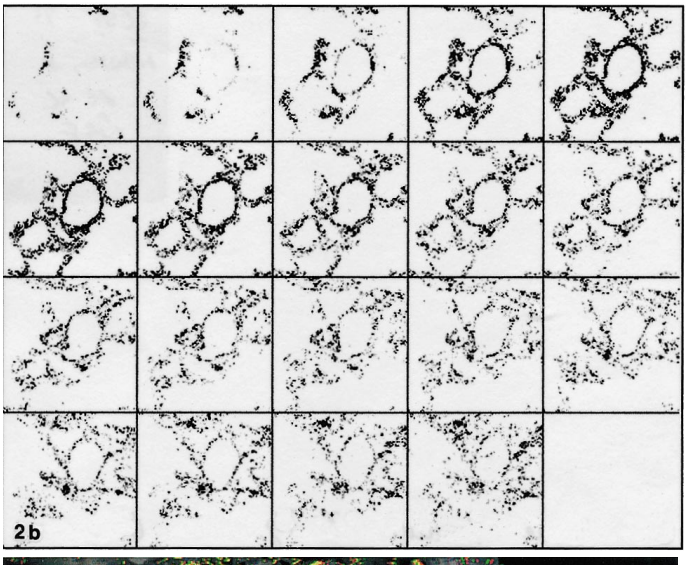

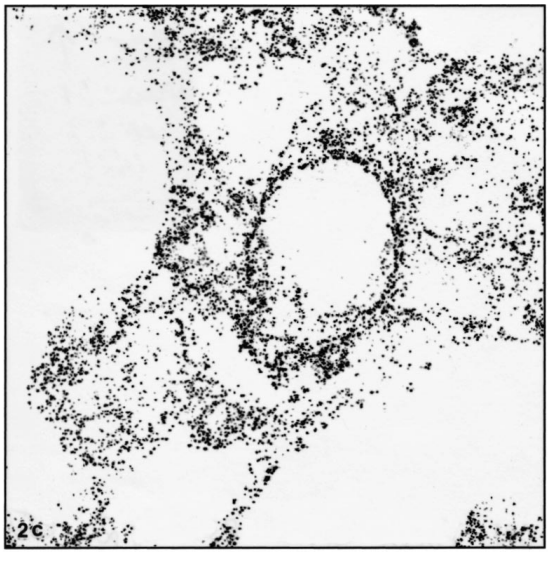

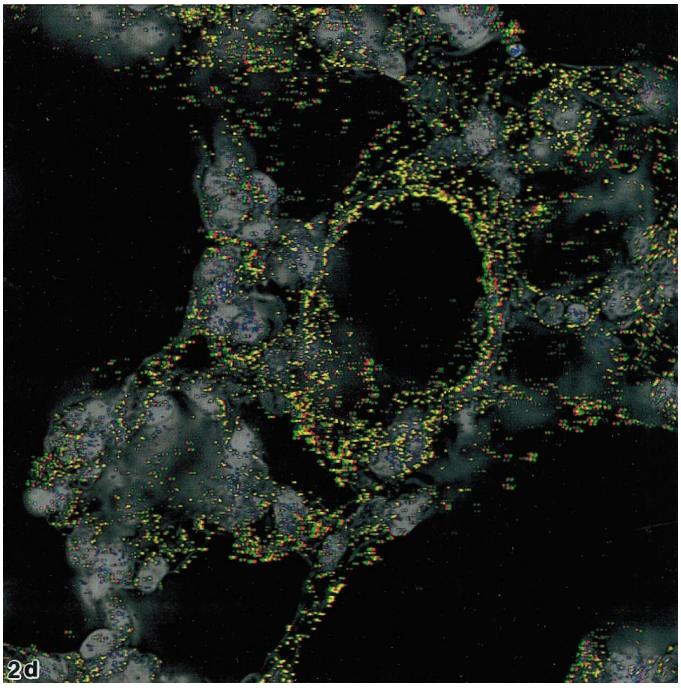

Fig. 2a–d The same section as shown in Fig. 1 electronically imaged in the confocal laser scanning microscope (CLSM). **a** An image from the transmitted laser light detector below the specimen stage. As with bright-field microscopy, visualisation of the immunostain depends on focal plane (*as* air space, *C* capillary lumen). *Scale bar* 20 μm. **b** A gallery of 19 optical sections taken at steps of 0.46 μm through the paraffin section with the CLSM set to record reflection images. The very reflective particles of dense gold/silver immunostain are shown in *black*. The linearity of the immunostain is apparent in many of the sections. **c** An extended focus image of all 19 optical sections shown simultaneously. The total amount of immunostaining can now be seen. Some linearity is still apparent but with no lung structure visible its significance cannot be properly assessed. **d** A red/green stereo reconstruction of the 19 optical sections shown in **b**. The transmission image shown in **a** has been inverted and ghosted over the stereo reconstruction to provide a background of lung architecture against which to evaluate the immunostaining. The image when viewed through red/green stereo glasses shows the three-dimensional reconstuction of the whole 10-μm paraffin section including all of the immunostaining. The nuclei and some of the cell profiles are shown overlaid in light grey

Western blot determination of caveolin expression in rat lung

To examine rat tissues for caveolin-1 expression, approximately 200 mg various rat organs, including lung, were harvested and processed in immunoprecipitation buffer [1% Triton X-100; 60 mM octyl-glucoside; 150 mM NaCl; 20 mM TRIS pH 8.0; 2 mM ethylenediaminetetraacetate (EDTA); 50 mM NaF; 30 mM Na pyrophosphate; 100 μM Na orthovanadate; 1 mM phenyl methyl sulphonyl fluoride (PMSF) and 2 μg/ml leupeptin] to extract protein. Tissue lysates were clarified by centrifugation at 3000 *g* for 45 min and the protein content of the supernatant determined (Lowry et al. 1951). Lysate supernatants were diluted 1:10 with x2 electrophoresis sample buffer [x1=125 mM TRIS-HCl, pH 6.8, 2% sodium dodecyl sulphate (SDS), 5% glycerol, 0.003% bromophenol blue, and 1% ß-mercaptoethanol], and aliquots equivalent to 100 μg total protein per sample were resolved in a 15% SDS/polyacrylamide gel using the method of Laemelli (1970). Gels were electroblotted to polyvinyldene difluoride (PVDF) membrane (Biorad UK) and the membrane probed with 1:4000 dilution of the primary antibody, rabbit anti-caveolin-1. After a 18-h incubation at 4°C, the membrane was washed and probed with the secondary antibody, an anti-rabbit horseradish-peroxidase-conjugated IgG. Incubation proceeded for 1 h, after which the membrane was washed and chemiluminescent signal generated by use of an enhanced chemiluminescence (ECL) kit (Amersham UK) and captured and quantified on film by densitometry.

Results

Discrete sites of immunostaining in rehydrated paraffin wax sections of glutaraldehyde-fixed rat lung tissue were convincingly demonstrated without the need for any antigen retrieval methods. The specificity of the polyclonal antibody was validated by controls which were consistently negative, and dilution profiles in which non-specific background immunostaining was shown only at the higher antibody concentrations. In wet preparations, during silver intensification, it was extremely difficult to detect the marker microscopically which made it necessary to compare different times of silver development. At dilutions in excess of 1:1000 of the primary antibody, in optimally intensified sections, there was widespread tissue staining with little non-specific background. However, in bright-field microscopy, even though the sections were only 5 or 10 μm thick, it was extremely difficult to assess the structural localisation of the very finely distributed immunomarker because so little of it could be seen in any one focal plane (Fig. 1). A similar problem was observed in the CLSM when using the transmitted laser light detector below the specimen stage (Fig. 2a), but these images provided structural information, for example on the position of the cell nuclei. The gold/silver marker was particularly appropriate for reflection mode CLSM. Galleries of optical sections of the immunostained tissue at less than 0.4 μm distance apart (Fig. 2b) revealed the fine linearity of the immunomarker in particular along the thin membranes of the alveolar epithelium and capillary endothelium. Extended focus views of all the optical sections in a gallery superimposed (projection maximum) confirmed the high immunoresponse by showing the whole 5–10 μm depth of the section at once (Fig. 2c). However, only three-dimensional reconstructions gave a view of both total immunostaining and its localisation to lung membranes, the convolutions of which were surprisingly complex in such thin slices of tissue. Ghosted transmission images shown over red/green stereo pairs provided architectural detail (Fig. 2d) so that in the three-dimensional reconstruction the alveolar spaces were more easily identified and separated from blood spaces, enabling identification of the positive immunostaining of the alveolar membranes.

Electron microscopy afforded greater structural detail of the alveolar epithelial-capillary endothelial barrier. Postfixing the tissue in osmium retained the fine morphologic structure of the barrier. Figure 3a shows a section away from the nuclear region consisting of the very thin (150–200 nm) cytoplasmic attenuations of an ATI cell on the air-space side with a similarly thin extension of endothelial cell cytoplasm on the capillary lumen side. The two can be seen separated by a basement membrane with the thickness of the whole barrier constituting no more than 0.5 μm. Flask-shaped invaginations morphologically indicative of caveolae can be seen in both the ATI and capillary endothelial cell but, consistent with previous morphologic studies (Gil et al. 1981; Gil 1983), were more numerous in the endothelial cell. Postfixation in osmium and embedding in epoxy resin were incompatible with caveolin immunolabelling. However, antigenicity was retained if osmium was avoided and an acrylic resin such as LR White was employed (Fig. 3b,c). Figure 3b shows an LR White thin section of an attenuated region of the lung alveolar-capillary barrier similar to that shown in Fig. 3a. Both the ATI epithelium and endothelium displayed anti-caveolin immunogold labelling with, in general, particle frequency greater in the endothelium than in the epithelium. Taking the size of antibodies into account, the resolution of colloidal gold to specific membrane profiles should be within a proximity averaging 10–30 nm. In both cell types cytoplasmic vesicles and flask-shaped membrane indentations could be identified that were decorated with anti-caveolin-1 immunogold label. In Fig. 3c the functional unit of the lung alveolar pulmonary capillary barrier can be seen, with specific immunolabelling in both ATI and endothelial cells, but also evident in the cuboidal alveolar epithelial type II cell. A thorough examination of a large number of tissue sections failed to reveal structures in the ATII cell with the morphologic appearance of caveolae. A consistent finding also shown in Fig. 3c was of more intense labelling at sites proximal to the intercellular junctions between ATII and ATI cells. Figure 3c (inset) emphasises that not all cellular invaginations that are morphologically consistent with caveolae are decorated with anti-caveolin-1 immunogold label. This can also be seen in Fig. 3b and was equally applicable to both ATI epithelial and pulmonary capillary endothelial cells.

Western blot analysis for caveolin-1 in various tissues of the rat revealed strong expression in the lung (Fig. 4). For direct comparison each lane was loaded with a fixed amount of tissue extracted total protein, i.e., 100 μg total protein per sample. The MDCK cells are a recognised positive control for caveolin-1 in Western blot analysis. Expression was strongest in fat and lung tissue, with the signal

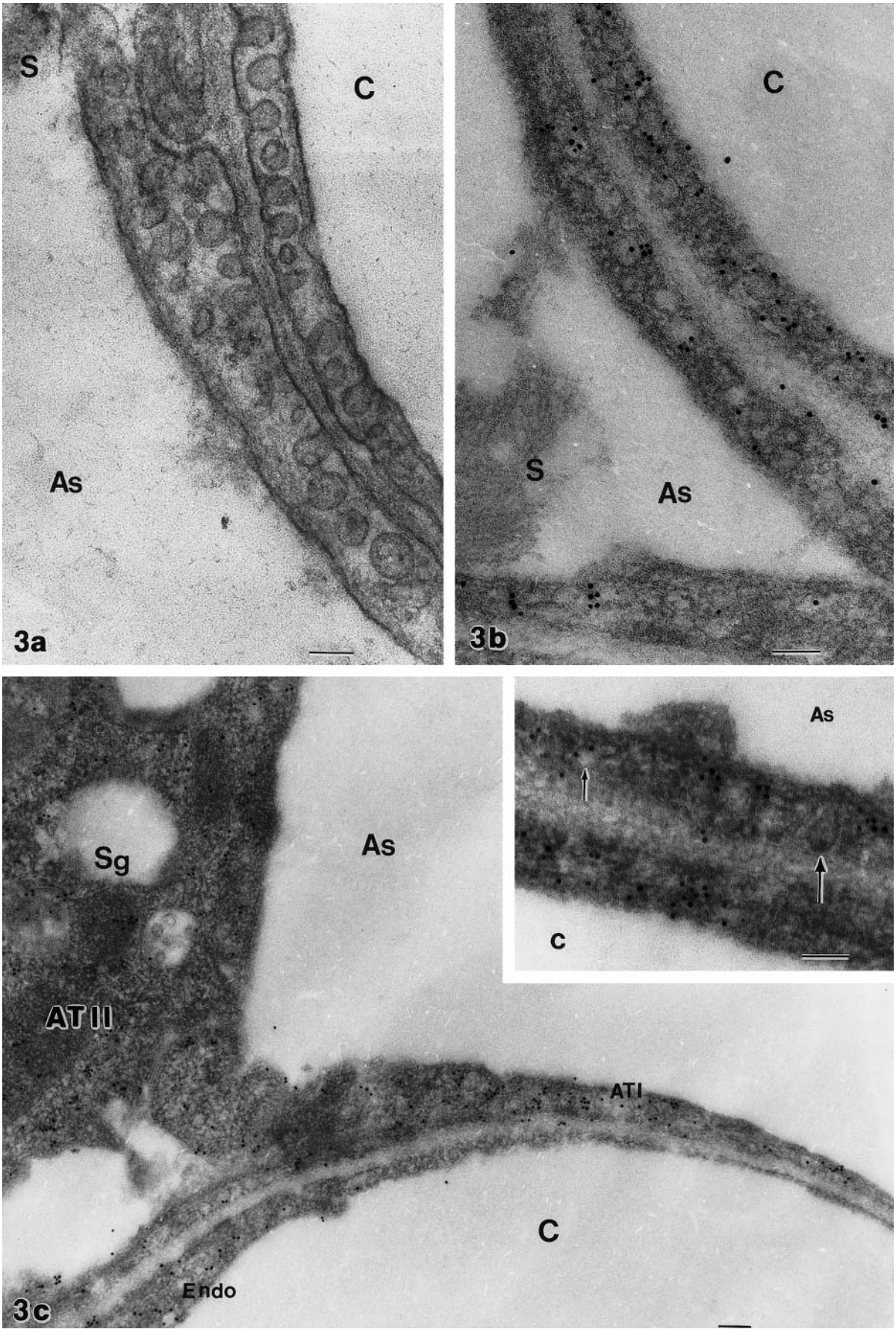
S
C
As
3a
C
S
As
3b
Sg
As
ATII
As
C
ATI
C
Endo
3c

for lung 71% of that for fat. Under the conditions of analysis no detectable signal was obtained for thymus, kidney, spleen and liver.

Discussion

Using immunocytochemical techniques this study has shown specific signal for caveolin-1 in the attenuated regions of the in vivo ATI cell. The antibody utilised does not distinguish between caveolin isoforms 1α and 1β. However, evidence collected using in-house isoform-specific antibodies indicates that with constitutive and recombinant caveolin-1-expressing cell lines the subcellular distributions of 1α and 1β isoforms largely overlap with both isoforms colocalising to caveolae (Sherer et al. 1995).

Both light- and electron-microscopic techniques were essential to characterise the antibody reactions and provide unambiguous cellular and subcellular localization of caveolin immunomarker. Monoclonal (host: mouse) and polyclonal (host: rabbit) commercially available anti-caveolin-1 antibodies were tested as part of pilot immunocytochemical validation studies. These studies were undertaken using rehydrated paraffin wax sections of rat lung. Initially, tissue was prepared following a number of fixation methods including neutrally buffered formalin, mixtures of formalin and glutaraldehyde, and glutaraldehyde on its own, and using both immersion and perfusion methods. In the absence of antigen retrieval methods, which were omitted because we intended to develop the chosen regime ultrastructurally, only the polyclonal antibody gave consistent, specific, high-affinity immunostaining across the whole range of fixed lung tissues (data not shown). This contrasts with the findings of Brown et al. (1996) and Kasper et al. (1998), who describe the need for antigen retrieval methods to restore antigenicity toward caveolin. Following paraffin wax embedding, lung tissue perfusion-fixed with glutaraldehyde gave us the finest structure and the sharpest antibody localisation in the light microscope, and similarly fixed tissue was adopted for embedding into both epoxy and acrylic resins for the electron microscope. Immunocolloidal gold was preferred as a marker because its amplification with a powerful new physical developer (Newman and Jasani 1998 in press) gave dense, punctate immunostaining with low background. When compared with controls, unequivocal immunolabel was seen in experimental tissue by bright-field light microscopy of immunostained paraffin sections, but the gold/silver marker was often very fine and difficult to image with only some of it appearing in any one plane of focus. However, its high reflectivity made it ideal for CLSM, which resolved more signal than was optically visible by bright-field microscopy. Image galleries of optical sections less than 0.5 μm in thickness taken through the 10-μm-thick immunostained paraffin sections showed an increased laser signal and higher resolution, making the linearity and membrane distribution (airspace vs capillary lumen) of the marker much clearer. However, only when galleries were reconstructed as three-dimensional images could both the total immunostaining and its distribution be fully appreciated on lung membranes. Specifically, three-dimensional reconstructions revealed the convoluted nature of the thin alveolar epithelial and capillary endothelial barriers even in tissue sections of only 5–10 μm thickness. With the profile of alveolar membranes identified, the positive immunostaining of alveolar epithelium as distinct from the capillary endothelium (recognised to be caveolin-rich) could be corroborated. A recent study (Kasper et al. 1998) employing double immunofluorescence labelling of embedded lung sections has also claimed caveolin localisation specifically to the ATI cell. However, our CLSM studies showing the convoluted nature of the lung alveolar membranes, even within the high resolution of paraffin wax sections 5–10 μm thick, lead to a considerable degree of uncertainty as to the precision with which these workers were able to differentiate between caveolin signal from alveolar epithelial or capillary endothelial sources. Further, we have found considerable nonspecific labelling when using the elevated antibody concentrations (1:20 to 1:40 dilution of polyclonal) as described by Kasper et al. (1998).

Transmission electron microscopy (TEM) provided unequivocal cellular identity for caveolin signal and was essential to delineate caveolin subcellular localisation within cells of the lung alveolar-capillary barrier. Caveolae were clearly resolvable by TEM with glutaraldehyde fixation and postfixation in osmium to preserve membrane structure. However, even after etching the epoxy resin sections in hydrogen peroxide (Baskin et al. 1979) or the unmasking of epitopes by removal of osmium with sodium metaperiodate (Bendayan and Zollinger 1983), we observed only non-specific background labelling (data not presented). In acrylic resin embedded lung tissue, where postfixation in osmium was substituted with uranyl acetate, good immunolabelling was, however, achieved without etching, although mem-

Fig. 3a–c Transmission electron micrographs of resin-embedded lung tissue (*As* air space, *C* capillary lumen). *Scale bars* 100 nm. **a** Araldite thin section of tissue postfixed in osmium showing the alveolar-pulmonary capillary barrier in rat lung. Micrograph shows flask-shaped plasmalemmal invaginations and cytoplasmic vesicles in both capillary endothelium (*right-hand surface*) and alveolar type I (ATI) epithelium (*left-hand surface*). They are separated by a prominent basement membrane. Note also in the airspace the presence of surfactant (*S*). **b** LR White thin section (osmium omitted) immunolabelled for caveolin-1. An attenuated region similar to that in **a** showing numerous colloidal gold particles associated with plasmalemma invaginations (morphologically characteristic of caveolae) and cellular vesicles in both ATI and endothelial cells. The epithelial surface is identified by surfactant (*S*). **c** LR White thin section immunolabelled as in **b** and showing the functional unit of the lung alveolar pulmonary capillary barrier. An alveolar type II cell (*ATII*) containing surfactant granules (*Sg*) abuts against the attenuated cytoplasm of an alveolar type I (*ATI*) cell. The capillary space (*C*) is lined with equally attenuated endothelium (*Endo*). Specific colloidal gold labelling is seen in both endothelium and *ATI* cell cytoplasm. Note caveolin immunolabelling of the *ATII* cell and the high frequency of labelling at *ATI-ATII* junctions. *Inset* Classically shaped caveolae invaginations shown in an *ATI* cell. A basal-orientated invagination is displayed associated with immunolabelling (*small arrow*), and an apical-orientated invagination is seen which lacks immunolabel (*large arrow*)

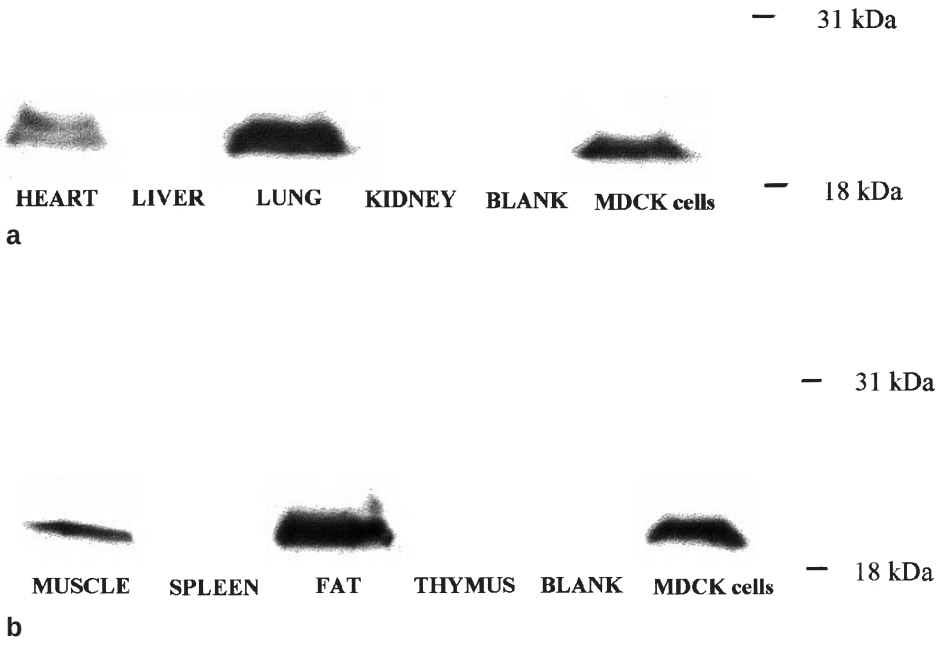

Fig. 4a,b Western blot analysis of various rat tissues for caveolin-1 revealing strong expression in the lung and fat. Each lane was loaded with 100 µg of tissue-extracted total protein. MDCK cells are a positive control for caveolin-1. No detectable signal was obtained for thymus, kidney, spleen and liver

brane definition was less well preserved. Nevertheless, sufficient morphology was retained to identify cytoplasmic vesicles and flask-shaped membrane invaginations in the attenuated regions of both the endothelial and ATI cells. Both the ATI epithelium and endothelium displayed specific anti-caveolin immunogold labelling. Concordant with the observed higher numerical density of caveolae, the immunogold particle frequency was, in general, greater in the endothelium than in the epithelium. Intriguingly, we have consistently observed a higher frequency of membrane invaginations and caveolin immunolabelling at sites proximal to ATII–ATI tight-junctional complexes, an observation which may not be unrelated to that of Rothberg et al. (1992) describing a higher density of caveolae at the migrating edge of cultured fibroblasts. However, the significance of this remains to be ascertained.

Consistent with a role for caveolae vesicles as a component of a cell's sorting and intracellular trafficking machinery, caveolin dynamics involves transport between plasmalemma and trans-Golgi network (Dupree et al. 1993). In the thin cytoplasmic attenuations at the periphery of the ATI cell there is a deficiency of tangible Golgi apparatus and therefore immunolabelling at these sites may be interpreted as emanating from caveolin-rich domains within the plasmalemma, caveolae invaginations and free caveolae cytoplasmic vesicles. This is substantiated by examination of the distribution of caveolin immunomarker with respect to subcellular morphology. In both ATI and endothelial cells, profiles of cytoplasmic vesicles and membrane invaginations were seen decorated with anti-caveolin-1 immunogold label. Coexistent with this, in both the aforementioned cell types could be seen flask-shaped membrane invaginations that lacked associated caveolin immunogold label. This could reflect a true biochemical heterogeneity in populations of morphologically similar plasmalemmal invaginations. Plasmalemma invaginations morphologically consistent with caveolae have previously been shown in preparations from a caveolin-negative cell line (Sargiacomo et al. 1993; Zurzolo et al. 1994). Alternatively, it could reflect an antigen threshold requirement coupled with a continuous variability in the level of caveolin membrane association, or indeed of epitope access arising during tissue processing.

Caveolae are enriched in sphingomyelin, glycosphingolipids and cholesterol, and the interaction between lipids, particularly cholesterol, and oligomeric caveolin complexes fulfils a critical role in the generation of caveolae structure (Monier et al. 1996). Although caveolin may not be the only essential element in the formation of caveolae, its requirement is nevertheless most readily demonstrated by studies showing: the parallel induction of caveolin-1 expression and of caveolae formation during differentiation of 3T3-L1 adipocytes (Fan et al. 1983; Scherer et al. 1994); the respective parallel loss in oncogenically transformed cells (Koleske et al. 1995); and recombinant expression of caveolin-1 in caveolin-negative cells driving the de novo formation of caveolae (Li et al. 1996; Fra et al. 1995). Our observations of specific labelling with caveolin immunomarker in the cuboidal alveolar epithelial type II cell (ATII) despite ultrastructural evidence for a lack of caveolae in this cell type support the assumption that factors in addition to that of caveolin are required for the generation of caveolae. Indeed, consistent with ATII in vivo data, in vitro data from our own laboratory (unpublished) show a weak, but nevertheless positive, signal for caveolin-1 in Western blots of a human ATII cell line, A549, which lack caveolae structures.

With ATII and ATI cells staining positive for caveolin (as demonstrated in the current study) and with the

recognised expression of caveolin in capillary endothelial cells, over 50% of the cell population of lung parenchyma is caveolin-positive. Not surprisingly therefore Western blot data confirm extensive caveolin expression in lung tissue. Northern blot analysis of rat tissues has previously shown caveolin-1 mRNA in fat, lung and skeletal muscle, but not kidney, liver or spleen (Tang et al. 1996). The latter report indicated that caveolin-1 mRNA in skeletal muscle reflects that associated with the endothelial cells within the tissue and not the muscle fibres themselves. The lack of caveolin-1 signal arising from endothelium within organs such as liver, spleen and kidney may reflect the phenotypic heterogeneity recognised for endothelium and the nature of predominant capillary endothelial cell within that particular tissue (Simionescu and Simionescu 1991).

The functions of caveolae in a range of cell types are under intense investigation. The range of proteins reported to be associated with caveolae is extensive and continues to grow (see reviews of Lisanti et al. 1994 and Couet et al. 1997) and includes among others: signalling molecules such as Gα-subunits; endothelial nitric-oxide synthase; G-protein-coupled receptors such as endothelin receptor; growth-factor receptors such as that for insulin; and channels such as an inositol triphosphate sensitive Ca^{2+} channel. However, caveolae may not perform the same function(s) in all cell phenotypes in which this structure has been identified (Anderson 1993). It therefore follows with biochemical confirmation that at least some of the invaginations/vesicles in the ATI cell fulfil the biochemical definition of caveolae, and that the function(s) of these structures within alveolar epithelium should now be specifically addressed.

The numerical densities of morphologically recognisable caveolae in the ATI cell have been variously determined at 145–260/μm^3 ATI cell volume through to 150–250/μm^2 ATI cell surface (DeFouw and Chinard 1982; DeFouw 1983; Gil et al. 1981). Given the dimensions of the human ATI cell (Crapo et al. 1982), the above determinations would equate to 0.4–1.9x10^6 caveolae invaginations/caveolae vesicles per ATI cell at 'steady-state'. Regulation of alveolar protein clearance in the uninjured lung is a necessary process (Folkesson et al. 1996) and, drawing parallels with endothelial caveolae, one of the most apparent functions that could be envisioned for ATI caveolae is that of protein transport. In capillary endothelium a primary function of caveolae has long been considered the fluid-phase endocytosis of plasma macromolecules (Silverstein et al. 1977; Schneeberger 1983). More recent studies on the endocytic and transcytotic functions of capillary endothelial caveolae (Schnitzer and Oh 1994; Schnitzer et al. 1994) have observed that endothelial caveolae mediate the endocytosis of modified albumins via receptor-mediated (gp30 and gp18) internalization. These modified albumins are then directed to endosomes and lysosomes for degradation, and thereby a caveolae-scavenging function is provided. Further, endothelial caveolae have been implicated in the receptor-mediated (gp60) internalization and transcytosis of native unmodified albumin. A protein trafficking function for ATI cell caveolae has implications beyond that of a constitutive role, for example in both the initiation and resolution phases of pulmonary oedema. Indeed, morphometric EM studies in the late 1970s (DeFouw and Berendsen 1978; DeFouw and Berendsen 1979) demonstrated that in animal models of permeability-induced pulmonary oedema increases of 200–300% in the number of what are now recognised as caveolae could be observed in both the ATI cell and the pulmonary capillary endothelial cell without concomitant changes in caveolae size or indeed cell thickness. Such an increase in caveolae number could be under control of chemical signals as described recently by the study of Senda et al. (1997), who demonstrated in an osteoblastic cell line that a dermonecrotizing toxin which activates the GTP-binding protein, Rho, leads to increased caveolae formation. Caveolae-mediated protein transport is also of interest not least to pharmaceutical researchers aiming to exploit alveolar epithelial transport mechanisms to deliver more efficiently therapeutic proteins and peptides via lung inhalation to the systemic circulation (Patton and Platz 1992; Patton 1996). Clearly, the potential range of functions for ATI caveolae extend beyond protein transport per se, and the specific interactions of these structures with the alveolar environment require further study.

In conclusion, this study has detailed with immunocytochemical techniques that at least certain populations of the plasmalemmal invaginations and cytoplasmic vesicles in the ATI cell in vivo are associated with caveolin-1, and as such biochemically conform to the definition of caveolae. Such biochemical characterisation affords the development of understanding about caveolae function derived from a range of studies conducted in different cell phenotypes and has broad implications for the assignment and further study of ATI cell functions, including the role of ATI caveolae in signal transduction and in macromolecule trafficking across alveolar epithelium.

Acknowledgements The authors would like to acknowledge Mrs. E.M.V. James, Miss A. Oversby and Dr. J.A. Hobot from the UWCM Medical Microscopy Unit, and Mr. A. Al-Eid, Mr. A. Al-Wan, Mr. K. Ritchie and Mr. A. Hollins from UWC for fruitful discussions and excellent assistance.

References

Anderson RGW (1993) Plasmalemmal caveolae and GPI-anchored membrane proteins. Curr Opin Cell Biol 5:647–652

Anderson RGW, Kamen BA, Rothberg KG, Lacey SW (1992) Potocytosis: sequestration and transport of small molecules by caveolae. Science 255:410–411

Baskin DG, Erlandsen SL, Parsons JA (1979) Influence of hydrogen peroxide or alcoholic sodium hydroxide on the immunocytochemical detection of growth hormone and prolactin after osmium fixation. J Histochem Cytochem 27:1290–1292

Bendayan M, Zollinger M (1983) Ultrastructural localization of antigenic sites on osmium-fixed tissues applying the protein A–gold technique. J Histochem Cytochem 31:101–109

Brown J, Lydon J, McLaughlin M, Tilley A, Tyszkowski R, Alper S (1996) Antigen retrieval in cryostat sections and cultured cells by treatment with sodium dodecyl sulphate (SDS). J Histochem Cell Biol 105:261–267

Bungard M, Frokjaer-Jensen J, Crone C (1979) Endothelial plasmalemmal vesicles as elements in a system of branching in-

vaginations from the cell surface. Proc Natl Acad Sci USA 76:6439–6442
Couet J, Li S, Okamoto T, Scherer PE, Lisanti MP (1997) Molecular and cellular biology of caveolae. Paradoxes and plasticities. Trend Cardiovas Med 7:103–110
Crapo JD, Barry BE, Gehr P, Bachofen M, Weibel ER (1982) Cell number and cell characteristics of normal human lung. Am Rev Respir Dis 125:332–337
DeFouw DO (1983) Ultrastructural features of alveolar epithelial transport. In: Crandell E (ed) Fluid balance across alveolar epithelium. Am Rev Res Dis 127 (Suppl): S9–S14
DeFouw DO, Berendsen PB (1978) Morphologic changes in isolated perfused dog lungs after acute hydrostatic edema. Circ Res 43:72–82
DeFouw DO, Berendsen PB (1979) A morphometric analysis of isolated perfused dog lungs after acute oncotic edema. Microvasc Res 17:90–103
DeFouw DO, Chinard FP (1982) Numerical densities of cellular vesicles in pulmonary alveolar septa of edematous dog lungs. Microvasc Res 23:248
Dupree P, Parton RG, Raposo G, Kurzchalia TV, Simons K (1993) Caveolae and sorting in the trans-Golgi network of epithelial cells. EMBO J 12:1597–1605
Fan JY, Carpentier J-L, van Obberghen E, Grunfeld C, Gorden P, Orci L (1983) Morphological changes of the 3T3-L1-fibroblast plasma membrane upon differentiation to the adipocyte form. J Cell Sci 61:219–230
Fawcett DW (1966) The cell. Saunders, Philadelphia
Fielding PE, Fielding CJ (1996) Intracellular transport of low density lipoprotein derived free cholesterol begins at clathrin-coated pits and terminates at cell surface caveolae. Biochemistry 35:14932–14938
Folkesson HG, Matthay MA, Westrom BR, Kim KJ, Karlsson BW, Hastings RH (1996) Alveolar epithelial clearance of protein. J Appl Physiol 80:1431–1445
Fra AM, Williamson E, Simons K, Parton RG (1995) De novo formation of caveolae in lymphocytes by expression of VIP21-caveolin. Cell Biol 92:8655–8659
Glauert AM (1991) Epoxy resins: an update on their selection and use. Microsc Anal 25:15–20
Gil J (1983) Number and distribution of plasmalemma vesicles in the lung. Fed Proc 42:2414–2418
Gil J, Silage DA, McNiff JM (1981) Distribution of vesicles in cells of the air-blood barrier in the rabbit. J Appl Physiol 50:334–340
Glenney JR, Soppet D (1992) Sequence and expression of caveolin, a protein component of caveolae plasma membrane domains phosphorylated on tyrosine in Rous sarcoma virus-transformed fibroblasts. Proc Natl Acad Sci USA 89:10517–10521
Haies DM, Gil J, Weibel ER (1981) Morphometric study of rat lung cells: numerical and dimensional characteristics of parenchymal cell populations. Am Rev Respir Dis 123:533–541
Kasper M, Reimann T, Hempel U, Wenzel K-W, Bierhaus A, Schuh D, Dimmer V, Haroske G, Muller M (1998) Loss of caveolin expression in type I pneumocytes as an indictator of subcellular alterations during lung fibroblasts. Histochem Cell Biol 109:41–48
Koleske AJ, Baltimore D, Lisanti MP (1995) Reduction of caveolin and caveolae in oncogenically transformed cells. Proc Natl Acad Sci USA 92:1381–1385
Kurzchalia TV, Parton RG (1996) Are they still moving: dynamic properties of caveolae. FEBS Lett 389:52–54
Laemelli UK (1970) Cleavage of structural proteins during the assembly of the head of bacteriophage T4. Nature 227:680–685
Li S, Song KS, Koh S, Kikuchi A, Lisanti MP (1996) Baculovirus-based expression of mammalian caveolin in Sf21 insect cells: a model system for the biochemical and morphological study of caveolae biogenesis. J Biol Chem 271:28647–28654
Lisanti MP, Scherer P, Tang Z, Sargiacomo M (1994) Caveolae, caveolin and caveolin-rich membrane domains: a signalling hypothesis. Trend Cell Biol 4:231–235
Lowry OH, Rosebrough NJ, Farr AL, Randell RJ (1951) Protein measurement with the Folin phenol reagent. J Biol Chem 139:190–198
Monier S, Dietzen DJ, Hastings WR, Lublin DM, Kurzchalia TV (1996) Oligomerization of VIP21-caveolin in-vitro is stabilised by long chain fatty acylation or cholesterol. FEBS Lett 388:143–149
Newman GR, Hobot JA (1987) Modern acrylics for post-embedding immunostaining techniques. J Histochem Cytochem 35:971–981
Newman GR, Hobot JA (1993) Resin microscopy and on-section immunocytochemistry. Springer-Verlag, Berlin Heidelberg New York
Newman GR, Jasani B (1998) Silver development in microscopy and bioanalysis: a new versatile formulation for modern needs. Histochem J (in press)
Parton RG, Joggerst B, Simons K (1994) Regulated internalization of caveolae. J Biol Chem 127:1199–1215
Patton JS (1996) Mechanisms of macromolecule absorption by the lungs. Adv Drug Deliv Rev 19:3–36
Patton JS, Platz RM (1992) Pulmonary delivery of peptides and proteins for systemic action. Adv Drug Deliv Rev 8:179–196
Reynolds ES (1963) The use of lead citrate at high pH as an electron-opaque stain in the electron microscope. J Cell Biol 17:208–212
Rothberg KG, Heuser JE, Donzell WC, Ying Y, Glenney JR, Anderson RGW (1992) Caveolin, a protein component of caveolae membrane coats. Cell 68:673–682
Sargiacomo M, Sudol M, Tang ZL, Lisanti MP (1993) Signal transducting molecules and GPI-linked proteins form a caveolin-rich insoluble complex in MDCK cells. J Cell Biol 122:789–807
Scherer PE, Lisanti MP, Baldini G, Sargiacomo M, Mastick CC, Lodish HF (1994) Induction of caveolin during adipogenesis and association of GLUT4 with caveolin-rich vesicles. J Cell Biol 127:1233-1243
Scherer PE, Tang ZL, Chuns M, Sargiacomo M, Lodish HF, Lisanti MP (1995) Caveolin isoforms differ in their N-terminal protein sequence and subcellular distribution. J Biol Chem 270:16395–16401
Scherer PE, Okamoto T, Chun M, Nishimoto I, Lodish HF, Lisanti MP (1996) Identification, sequence, and expression of caveolin-2 defines a caveolin gene family. Proc Natl Acad Sci USA 93:131–135
Schneeberger EE (1983) Proteins and vesicular transport in capillary endothelium. Fed Proc 42:2419–2424
Schnitzer JE, Oh P (1994) Albondin-mediated capillary permeability to albumin. J Biol Chem 269:6072–6082
Schnitzer JE, Oh P, Pinney E, Allard J (1994) Filipin-sensitive caveolae-mediated transport in endothelium: reduced transcytosis, scavenger endocytosis and capillary permeability of select macromolecules. J Cell Biol 127:1217–1232
Senda T, Horiguchi Y, Umemoto M, Sugimoto N, Matsuda M (1997) *Bordetella bronchiseptica* dermonecrotizing toxin, which activates a small GTP-binding protein Rho, induces membrane organelle proliferation and caveolae formation. Exp Cell Res 230:163–168
Silverstein SC, Steinman RM, Cohen ZA (1977) Endocytosis. Rev Biochem 46:669–722
Simionescu M, Simionescu N (1991) Endothelial transport of macromolecules: transcytosis and endocytosis. Cell Biol Rev 25:1–80
Song KS, Scherer PE, Tang Z-L, Okamoto T, Li S, Chafel M, Chu C, Kohtz DS, Lisanti MP (1996) Expression of caveolin-3 in skeletal, cardiac and smooth muscle cells. J Biol Chem 271:15160–15165
Tang Z-L, Scherer PE, Okamoto T, Song K, Chu C, Kohtz DS, Nishimoto I, Lodish HF, Lisanti MP (1996) Molecular cloning of caveolin-3, a novel member of the caveolin gene family expressed predominantly in muscle. J Biol Chem 271:2255–2261
Way M, Parton RG (1995) M-caveolin, a muscle specific caveolin-related protein. FEBS Lett 376:108–112
Wu C, Butz S, Ying Y-S, Anderson RGW (1997) Tyrosine kinase receptors concentrated in caveolae-like domains from neuronal plasma membrane. J Biol Chem 272:3554–3559
Yohimura N, Murachi T, Heath R, Kay J, Jasani B, Newman GR (1986) Immunogold electron-microscopic localisation of calpain I in skeletal muscle of rats. Cell Tissue Res 224:265–270
Zurzolo C, van't Hof W, van Meer G, Rodriguez-Boulan E (1994) VIP21/caveolin, glycosphingolipid clusters and the sorting of glycosylphosphatidylinositol-anchored proteins in epithelial cells.